

Likelihood Analysis of the Local Group Acceleration

I. Schmoldt¹, E. Branchini², L. Teodoro²,
 G. Efstathiou³, C.S. Frenk², O. Keeble⁵, S. Maddox³, S. Oliver⁵,
 M. Rowan-Robinson⁵, W. Saunders⁴, W. Sutherland¹, H. Tadros⁶, S.D.M. White⁷

¹ *Department of Physics, University of Oxford, Keble Road, Oxford OX1 3RH, UK*

² *Department of Physics, University of Durham, South Road, Durham DH1 3LE, UK*

³ *Institute of Astronomy, University of Cambridge, Madingley Road, Cambridge CB3 0HA, UK*

⁴ *Institute for Astronomy, University of Edinburgh, Blackford Hill, Edinburgh EH9 3JS, UK*

⁵ *Imperial College of Science, Technology, and Medicine, Blackell Laboratory, Prince Consort Road, London SW1 2EZ, UK*

⁶ *Department of Physics, University of Sussex, Falmer, Brighton BN1 9QH, UK*

⁷ *Max Planck Institut für Astrophysik, Karl-Schwarzschild-Straße 1, 85740 Garching, Germany*

19 August 2019

ABSTRACT

We compute the acceleration on the Local Group using 11206 IRAS galaxies from the recently completed all-sky PSCz redshift survey. Measuring the acceleration vector in redshift space generates systematic uncertainties due to the redshift space distortions in the density field. We therefore assign galaxies to their real space positions by adopting a non-parametric model for the velocity field that solely relies on the linear gravitational instability and linear biasing hypotheses. Remaining systematic contributions to the measured acceleration vector are corrected for by using PSCz mock catalogues from N-body experiments.

The resulting acceleration vector points $\sim 15^\circ$ away from the CMB dipole apex, with a remarkable alignment between small and large scale contributions. A considerable fraction ($\sim 65\%$) of the measured acceleration is generated within $40 h^{-1}$ Mpc with a non-negligible contribution from scales between 90 and $140 h^{-1}$ Mpc after which the acceleration amplitude seems to have converged. The local group acceleration from PSCz appears to be consistent with the one determined from the IRAS 1.2 Jy galaxy catalogue once the different contributions from shot noise have been taken into account. The results are consistent with the gravitational instability hypothesis and do not indicate any strong deviations from the linear biasing relation on large scales.

A maximum-likelihood analysis of the cumulative PSCz dipole is performed within a radius of $150 h^{-1}$ Mpc in which we account for nonlinear effects, shot noise and finite sample size. The aim is to constrain the $\beta = \Omega^{0.6}/b$ parameter and the power spectrum of density fluctuations. We obtain $\beta = 0.70^{+0.35}_{-0.2}$ at 1σ confidence level.

The likelihood analysis is not very sensitive to the shape of the power spectrum due to the rise in the amplitude of the dipole beyond $40 h^{-1}$ Mpc and

due to the increase in shot noise on large scales. There is however a weak indication that within the framework of CDM models the observed Local Group acceleration implies some excess power on large scales.

Key words: Cosmology: theory – galaxies: clustering, – large-scale structure, large-scale dynamics.

1 INTRODUCTION

If the Cosmic Microwave Background [CMB] defines a cosmological frame, then the dipole pattern observed in its temperature is a direct measure, via Doppler shift, of the Local Group [LG] velocity: $v_c = 627 \pm 22 \text{ km s}^{-1}$ towards $(l, b) = (276^\circ \pm 3^\circ, 30^\circ \pm 2^\circ)$ as inferred from the 4-year-COBE data (Lineweaver *et al.* 1996). The best reason to prefer a velocity interpretation to more exotic scenarios (e.g. the Tolman-Bondi cosmological model of Paczynski & Piran 1990, where the dipole moment of the CMB is of cosmological origin) is the remarkable alignment of the dipole with the gravitational acceleration vector measured at the LG location. This gravitational acceleration is inferred from the distribution of luminous objects in our cosmological neighbourhood and is expected to align with the dipole vector within the Gravitational Instability (Peebles 1980) and linear biasing framework in which the observed structures in the universe grew via gravitational instability from initial small fluctuations in the mass density field. In the linear regime, i.e. on scales where the mass density contrast, δ_ρ , is small, we also expect a direct proportionality between the amplitudes of the two vectors. The proportionality constant is a measure of the so-called $\beta (= \Omega_m^{0.6} / b)$ parameter, where Ω_m represents the density and b , the bias parameter, relates the mass density contrast, δ_ρ , to the fluctuations in the number density of the luminous objects, $\delta_g = b\delta_\rho$. A comparison of the observed LG velocity with the gravitational acceleration is therefore a direct measure of β .

The many different estimates of the LG acceleration (see Strauss and Willick (1995) for a complete review) are partly contradictory. Most of the measurements agree in showing a small ($\leq 30^\circ$) misalignment between the CMB and the LG dipoles. The amplitudes, however, are highly sensitive to the objects used as mass tracers. As reported by Strauss (1997), the LG acceleration as calculated using galaxies extracted from the IRAS 1.2 Jy redshift survey (Fisher *et al.* 1995) and from the Optical Redshift Survey [ORS] (Santiago *et al.* 1995, 1996) seems to receive little contribution from scales larger than $40 h^{-1} \text{ Mpc}$. Other analyses carried out using a deeper but sparser redshift survey of IRAS galaxies, known as the QDOT catalogue, have shown a non-negligible contribution from scales up to $\sim 100 h^{-1} \text{ Mpc}$ (Rowan-Robinson *et al.* 1990). Clusters of galaxies, both optically and X-ray selected, can be used to probe very large scales because of their large luminosity. The LG gravitational acceleration generated by their spatial distribution also provides evidence of non-negligible contributions from depths up to $\sim 150 h^{-1} \text{ Mpc}$ (Scaramella, Vettolani & Zamorani 1991, Plionis & Valdarnini 1991, Plionis & Kolokotronis 1998).

Such an apparent dichotomy may arise from the limited depth of the ORS and IRAS 1.2 Jy catalogues, from the sparse sampling in the QDOT and cluster catalogues, or from inhomogeneity and observational biases that may affect the different samples.

In this paper, we use the recently completed PSCz survey of IRAS galaxies. This is a homogeneously selected all-sky catalogue which combines the depth of the QDOT with the dense sampling of the 1.2 Jy catalogue and therefore represents the ideal tool for investigating the large scale contribution to the LG gravitational acceleration. Our main concern is the combination of information on the growth of the dipole with other measurements of the local velocity fields (mainly from POTENT data) in a likelihood analysis and we therefore do not use the catalogue to its full extent. Rowan-Robinson *et al.* (1998) have done a careful analysis of the growth of the dipole on the largest scales using the same catalogue out to much larger distances.

Even with an ideal flux-limited catalogue, however, other effects (shot noise, finite depth of the sample, use of the linear approximation, incomplete sky coverage, and redshift space distortions) cause the LG acceleration to differ from the observed LG velocity, making it impossible to determine β by direct comparison. In this work, we adopt an alternative two-step procedure in which:

- the LG cumulative acceleration is computed from the data and its random and systematic errors are evaluated using PSCz mock catalogues extracted from N-body simulations. These catalogues are also used to statistically correct the measured PSCz dipole amplitude for systematic errors and to obtain a preliminary estimate of β from the data.
- the resulting bias-free gravitational acceleration is then analysed using a likelihood approach similar to the one developed by Strauss *et al.* (1992) [S92 hereafter]. This will yield an estimate of β within the framework of a given cosmology and a way of evaluating errors.

The outline of this paper is as follows: In §2 we give a short theoretical introduction. §3 is devoted to computing the LG acceleration from the data and to estimating numerical biases and errors with the help of mock catalogues. §4 contains a likelihood analysis (theory and application) of the results, and conclusions follow in §5.

2 THEORETICAL BACKGROUND

In linear theory, the peculiar velocity, \mathbf{v} , of a given galaxy is directly proportional to the gravitational acceleration, \mathbf{g} , caused by the surrounding matter. The two vectors are therefore parallel and related by

$$\mathbf{v}(\mathbf{r}) = \frac{H_0 f}{4\pi G} \mathbf{g}(\mathbf{r}), \quad (1)$$

where $f \sim \Omega_m^{0.6}$. Hence, if the peculiar velocity is known, Ω_m can be determined by calculating the gravitational acceleration from the observed mass distribution, where Ω_m is the density of all matter in units of the critical density.

During the past few years, particular attention has been paid to applying eqn. (1) to compute the acceleration acting on the Local Group of galaxies. The Local Group velocity in the CMB frame is accurately known from the CMB dipole anisotropy^{*} while the gravitational acceleration vector can be measured from redshift surveys which give an estimate of the three-dimensional galaxy density field. The vector \mathbf{g} is related to the mass density field by

$$\mathbf{g}(\mathbf{r}) = G \int \delta_\rho(\mathbf{r}') \frac{\mathbf{r}'}{|\mathbf{r}'|^3} d^3 \mathbf{r}' \quad (2)$$

where $\delta_\rho(\mathbf{r})$ is the density contrast at comoving coordinate \mathbf{r} . Since we sample the density contrast of the galaxy rather than of the matter distribution, we need to postulate some relation between the two. In this work, we assume linear biasing, in which $\delta_g = b\delta_\rho$, such that we can shift from galaxy to matter density simply by dividing by the bias factor b . Eqn. (1) then becomes

$$\mathbf{v} = \frac{H_0 \beta}{4\pi} \int d^3 \mathbf{r}' \frac{\mathbf{r}'}{|\mathbf{r}'|^3} \delta_g(\mathbf{r}'), \quad (3)$$

where $\beta = f/b$.

In principle, β can easily be obtained by comparing $|\mathbf{v}_r|$ and $|\mathbf{v}_c|$. In practice, however, the right hand side of eqn. (3) is difficult to evaluate from redshift surveys because of several effects:

- **Finite Sample Size:** The integral of equation 3 extends over all space. When using a redshift survey, however, this necessarily turns into a sum over a finite number of galaxies. The volume sampled extends to the maximum depth of the survey and excludes possible unsurveyed regions. Evaluating eqn. (3) in a finite survey volume results in a discrepancy between \mathbf{v}_r and \mathbf{v}_c .

- **Shot Noise:** At large radii, the sampling of the galaxy distribution becomes more and more sparse, which leads to an increase in the so-called shot noise error. In this work, the shot noise contribution is evaluated following the S92 approach, which also accounts for the uncertainty in the galaxy mass function, i.e. the uncertainty associated with the assumption that all galaxies have the same mass.

- **Redshift Space Distortions:** The surveys do not give full three-dimensional positions for the galaxies but rather angular positions and redshifts. Redshifts are related to distances via Hubble's law but only in the limit of very large distances. For nearby objects the peculiar velocities of the galaxies will add a significant contribution to the redshift that systematically distorts any density field calculated in redshift space (Kaiser 1987, Kaiser and Lahav 1988). We attempt to minimise redshift space distortions by reconstructing galaxy positions in real space from their redshifts.

- **Nonlinear Effects:** Eqn. (3) is not valid over the entire survey volume since linear theory breaks down in high density regions. Nonlinear contributions to peculiar velocities add incoherently to the vector, spoiling the linear relationship between velocity and acceleration vectors.

^{*} Note that both the CMB dipole and the gravitational acceleration caused by the surrounding matter are often referred to as 'dipoles'. In this paper we will obey this convention except when distinguishing between the 'CMB velocity' (\mathbf{v}_c), which is inferred from the CMB dipole anisotropy, and the 'measured velocity' (\mathbf{v}_r) inferred from the gravitational acceleration.

All these effects have to be accounted for before a meaningful statement can be made about the value of β calculated from a comparison of \mathbf{v}_r and \mathbf{v}_c . In what follows, we will use a likelihood analysis that models the non-linear effects and the finite survey volume. The shot noise contribution will be calculated directly from the data while a self-consistent dynamical algorithm is adopted to model the errors introduced when minimising redshift space distortions.

3 THE LOCAL GROUP ACCELERATION

In this section, we present the dataset used, our methods for calculating the dipole and for evaluating the associated errors and finally the results of these procedures. By using simulated redshift catalogues, we hope to be able to correct the calculated dipole for all those errors that cannot be accounted for in the likelihood analysis.

3.1 The Dataset

Our dataset comes from the recently completed IRAS PSCz catalogue – a redshift survey of some 15,500 galaxies detected in the IRAS Point Source Catalogue. The PSCz catalogue contains almost every galaxy in the IRAS PSC with 60 μm flux (f_{60}) larger than 0.6 Jy for which the redshift has been measured. Only sources from PSC with $f_{60} > 0.5f_{25}$ (to exclude stars) and with $f_{100} < 4f_{60}$ (to exclude most of the galactic cirrus) have been included in the catalogue. Our subsample contains 11206 PSCz objects within 200 h^{-1} Mpc, with PSC fluxes at 60 $\mu m > 0.6$ Jansky, and with positive galaxy identifications. Regions not surveyed by IRAS (two thin strips in ecliptic longitude and the area near the galactic plane defined by a V-band extinction of > 1.5 mag.) are excluded from the catalogue, which therefore covers $\sim 84\%$ of the sky.

We also consider a catalogue of galaxies extracted from the 1.2 Jy redshift survey (Fisher *et al.* 1995) which contains all the objects with $f_{60} > 1.2$ Jy, also within 20,000 km s^{-1} . The resulting 1.2 Jy subsample has $\sim 88\%$ sky coverage and contains 4626 galaxies.

3.2 Minimising Redshift Space Distortions

As outlined by Kaiser (1987) and Kaiser and Lahav (1988), redshift space distortions can modify the amplitude of the galaxy dipole, especially when it is measured from a flux-limited sample. To minimise this effect, we compute the galaxies' peculiar velocities and real space positions iteratively starting from the galaxy distribution as seen in the redshift space. A detailed methodological description can be found in Branchini *et al.* (1998), here we just summarise the main concepts. The method described is very similar to that developed by Yahil *et al.* (1991).

We assume linear GI and LB and look for an iterative solution to the system of equations

$$\mathbf{v}(\mathbf{r}) = \frac{H_0\beta}{4\pi} \int d^3\mathbf{r}' \frac{\mathbf{r}' - \mathbf{r}}{|\mathbf{r}' - \mathbf{r}|^3} \delta(\mathbf{r}') \quad (4)$$

and

$$\mathbf{r}_i = cz_i - \hat{\mathbf{r}} \cdot (\mathbf{v}_i - \mathbf{v}_c), \quad (5)$$

where \mathbf{v}_i is the peculiar velocity of the generic object i , \mathbf{v}_c is the LG velocity (both velocities are measured in the CMB frame), $\hat{\mathbf{r}}$ is the unit vector along the radial direction. Distances and velocities are expressed in km s^{-1} . The redshift z_i is measured in the LG frame. First, we make a guess for \mathbf{r} (which in the 0-th iteration coincides with the galaxy redshift), then compute $\mathbf{v}(\mathbf{r})$ from eqn. (4), correct to a new \mathbf{r} by eqn. (5) and continue the process until the calculated velocities \mathbf{v}_i converge. This is typically achieved within 8 iterations.

There are several additions to this, designed to minimise the uncertainties inherent in the procedure. When computing the gravitational acceleration from eqn. (4) we smooth the density field using a Top Hat window and a smoothing length equal to the average separation of objects at that distance. The minimum smoothing length is 5 h^{-1} Mpc to ensure sufficient smoothing even at distances where the interparticle separation is small. This procedure

mitigates nonlinear effects especially in high density environments but also impairs our ability to predict the small-scale features in velocity and density fields.

The free parameter β has to be determined *a posteriori* by comparing observations with model predictions. We adiabatically increase β from 0.1 to 1.0 in 10 iterations, thereby slowly increasing the effect of gravity to improve convergence of the velocity field (S92). The resulting peculiar velocities scale to first order in β which, as we will discuss in §3.4, causes the galaxy dipole to be almost independent of the β value used in the reconstruction.

The iterative procedure uses all the galaxies within $200 h^{-1}$ Mpc while the mass distribution beyond is considered to be homogeneous, i.e. we neglect its gravitational effect. This assumption is justified as long as the reconstruction is performed in the LG frame since relative peculiar velocities are not affected by external dipoles. Higher moments of external force fields only affect the reconstruction reliability in the outer regions. To avoid these edge effects we calculate peculiar velocities and real space positions only for galaxies out to $170 h^{-1}$ Mpc even though material out to $200 h^{-1}$ Mpc is considered to be gravitating. The error analysis in §3.4 indicates that the combined effect of shot noise and reconstruction uncertainties at that distance have already increased to over 30 % of the measured acceleration, so to maximise the reliability of the data, we perform the likelihood analysis only on data measured out to $150 h^{-1}$ Mpc.

Spurious gravitational acceleration may also arise if the galaxy sample does not have full sky coverage. To alleviate this effect, we fill the unobserved regions with synthetic objects using two distinct procedures: At high ($|b| \geq 8^\circ$) galactic latitude we fill the masked areas with a uniform distribution of simulated objects having the same average number density and selection function as the PSCz galaxies. At lower galactic latitudes ($|b| < 8^\circ$, the so called ‘zone of avoidance’) the masked area is filled with galaxies which are cloned from the PSCz galaxy distribution in two strips above and below the zone of avoidance (Yahil *et al.* 1991), also retaining PSCz galaxies with $|b| < 8^\circ$ at their observed position.

Since we are using a flux-limited catalogue, the number density of galaxies within the survey volume decreases with the distance. In the reconstruction we account for this effect by assigning a weight to each galaxy that is proportional to the inverse of the selection function at the position of the galaxy. Since the positions of the galaxies vary during the iterations, we recompute the selection function at each step from the observed galaxy fluxes using a parametric maximum likelihood technique, and the galaxy weights are updated accordingly. For the selection function we assume the analytic form proposed Yahil *et al.* (1991).

Most of the results presented here refer to this iterative reconstruction procedure. However, two other methods, fully described and tested in Branchini *et al.* (1998), have been implemented to check the robustness of the results. The first is a grid-based version of the above iterative method while the second is based on the Nusser and Davis approach (1994) that uses the first order Zel’dovich approximation to correct for redshift space distortions without any need for iterations. In what follows we will refer to these three methods as M1, M2 and M3. As we will show in §3.5, the PSCz dipoles reconstructed with the three methods are fully consistent with each other.

3.3 PSCz Mock Catalogues

Systematic uncertainties affecting the measured PSCz dipole have been evaluated using a series of PSCz mock catalogues. These were extracted from N-body simulations of CDM universes performed by Cole *et al.* (1998) using a $345.6 h^{-1}$ Mpc computational box. For the present analysis we have considered two of their cosmological models. They are:

- an $\Omega_m = 1$ CDM model with $\Gamma = 0.25$
- an $\Omega_\Lambda = 0.7$, $\Omega_m = 0.3$ CDM model

These two are flat CDM cosmologies normalised to reproduce the local abundance of clusters as explained in Eke, Cole, and Frenk (1996):

$$\begin{aligned} \sigma_8 &= 0.52\Omega_m^{-0.46+0.10\Omega_m} \text{ if } \Omega_\Lambda = 0, \text{ and} \\ \sigma_8 &= 0.52\Omega_m^{-0.52+0.13\Omega_m} \text{ if } \Omega_\Lambda = 1 - \Omega_m. \end{aligned}$$

The velocity fields of the N-body models have been smoothed with a top hat function of $1.5 h^{-1}$ Mpc to obtain pairwise peculiar velocities of $\sim 250 \text{ km s}^{-1}$ at $1 h^{-1}$ Mpc, a value close to that observed in the galaxy distribution (Guzzo *et al.* 1997, Strauss, Ostriker and Cen 1998). For each of the two models we produce 10 mock catalogues: We impose $b = 1$, a value compatible with the one commonly accepted for IRAS galaxies, in order to identify galaxies with particles in the simulations. The velocity field in each catalogue mirrors the conditions in the local universe: the central LG-like observer has a peculiar velocity of $\mathbf{v}_c = 625 \pm 25 \text{ km s}^{-1}$, the LG velocity residuals $\langle (v_i - v_c)^2 \rangle^{0.5}$ within $5 h^{-1}$ Mpc (sometimes called “shear”) are smaller than 200 km s^{-1} and the fractional overdensity within the same region is in the range $-0.2 < \delta < 1.0$ (Brown and Peebles 1987). Each catalogue has a depth of $170 h^{-1}$ Mpc (since our velocity analysis of the PSCz will only extend out to that distance) and the coordinate system is rotated such that the observer’s velocity vector points towards the observed CMB apex. Since the number density in the simulations ($\sim 0.039 h^3 \text{ Mpc}^{-3}$) is smaller than the one given by the PSCz selection function within $10.9 h^{-1}$ Mpc, we are forced to semi-volume limit our catalogues at that radius. At greater distances we use a Monte Carlo rejection technique to force the simulated galaxy population to obey the $N(z)$ distribution of PSCz galaxies. A random flux consistent with the selection function is then attributed to each galaxy. Finally, we mask the same areas as in the PSCz catalogue to mimic the incomplete sky coverage. A similar set of catalogues has been produced to mimic the galaxy distribution in the IRAS 1.2 Jy subcatalogue (§3.1). Given the smaller number density of 1.2 Jy galaxies (Fisher *et al.* 1995), the 1.2 Jy mock catalogues are semi-volume limited to a smaller radius of $7.8 h^{-1}$ Mpc.

3.4 Error Estimates Using Mock Catalogues

Several different effects prevent the reconstruction procedure from recovering the exact real space galaxy distribution and a less than perfect reconstruction generates both systematic and random errors in the dipole. S92 showed that the most serious systematic bias originates from the so called ‘rocket effect’ (Kaiser 1987, Kaiser and Lahav 1988) which represents the spurious acceleration measured from a magnitude-limited sample of galaxies by an observer with some peculiar velocity unconnected to the gravitational acceleration (e.g. an observer in a rocket). In our case the errors in the computed LG velocity mimic the non-gravitational acceleration. The characteristic signature of this effect is a monotonically increasing spurious contribution to the cumulative LG acceleration. S92 correct for this effect by modifying their reconstruction procedure. Here we adopt a different strategy which uses mock catalogues to correct not only for the rocket effect but also for further possible systematic effects that arise from filling the unsurveyed areas with synthetic objects. We consider a generic PSCz mock catalogue and measure the gravitational acceleration at the observer’s central position from the true, all-sky galaxy distribution in real space. We then measure the gravity vector from the same catalogue, after applying the filling procedure and after iteratively moving galaxies to their reconstructed real space positions. The two acceleration vectors are similarly affected by shot noise, finite sample size and nonlinear effects and thus any discrepancy can only be ascribed to the intrinsic uncertainties in the reconstruction, the filling techniques and to the rocket effect. For each of the mock catalogues we compute the vector difference between the two cumulative accelerations at different radii, thereby obtaining an estimate for the systematic dipole error. We then average the difference over the various catalogues of both cosmologies to account for our ignorance of the underlying, true cosmological model. The mean discrepancy represents the cumulative effect of the various systematic errors while the dispersion around the mean quantifies the random errors. A similar exercise has been performed using mock IRAS 1.2 Jy catalogues. Results of this procedure are displayed in figure 1. The points represent the systematic error on the cumulative dipole measured at a given radius whereas the errorbars display the dispersion in that error. Since we are showing a cumulative quantity, the errors on each shell are correlated, both in amplitude and direction. Note that v_{true} is the dipole velocity calculated using real space positions of galaxies, whereas v_{rec} is computed using the redshift space positions as described in §3.2. Both quantities are normalised to $\beta = 1$. Filled dots refer to PSCz mocks while small triangles refer an analogous analysis performed using the simulated IRAS 1.2 Jy catalogues.

It is encouraging to note that there is virtually no systematic error up to a distance of $150 h^{-1}$ Mpc. The marginal increase beyond that is probably the signature of the Kaiser effect. In what follows, the average systematic offset will

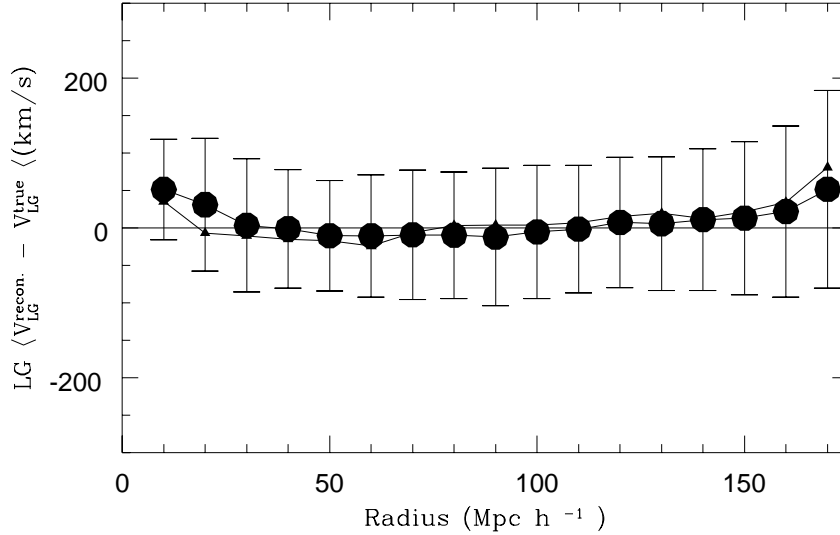


Figure 1. Error estimates from the mock catalogues. Black dots show the discrepancy between the true and the “observed” PSCz dipole, averaged over different mock catalogues at different radii. Error bars represent the scatter around the mean and quantify the amplitude of the random errors. Small triangles show similar results for the 1.2 Jy mock dipoles.

be subtracted out of the PSCz and IRAS 1.2 Jy dipoles to statistically correct for rocket-like effects. The importance of the different error sources seems to vary with the distance. In the inner regions nonlinear effects and intrinsic error in the reconstruction seem to dominate. Uncertainties in the filling procedures and Kaiser effect becomes dominant on larger scales. The former accounting for $\sim 40\%$ error budget at a distance of $100 h^{-1}$ Mpc, both in amplitude and direction. The typical random error on the differential dipole, α , amounts to $\sim 15 \text{ km s}^{-1}$ per shell of $10 h^{-1}$ Mpc. This error will be accounted for in the likelihood analysis of §4 in the same way as the shot noise.

The errors showed in figure 1 turned out to be Gaussian distributed around their mean (i.e. the black dots) which indicates that our error estimate, albeit based upon only 20 PSCz mock catalogs, are realistic. As outlined in §3.2, the reconstructed dipole scales with β linearly only to a first approximation. The actual result marginally depends on the value of β assumed in the reconstruction itself. To evaluate the amplitude of this effect we have performed 9 PSCz reconstructions varying β in the range $[0.4, 1.2]$, to include the range allowed by observations (see Dekel 1997). Figure 2 shows the average cumulative dipole from the 9 iterations. The upper and lower dashed lines display the dipoles for the $\beta = 1.2$ and $\beta = 0.4$, respectively. At the radius of $150 h^{-1}$ Mpc, the percentage difference is 11%, notably smaller than the 32% caused by the cumulative effect of random errors and shot noise. Also, note that the

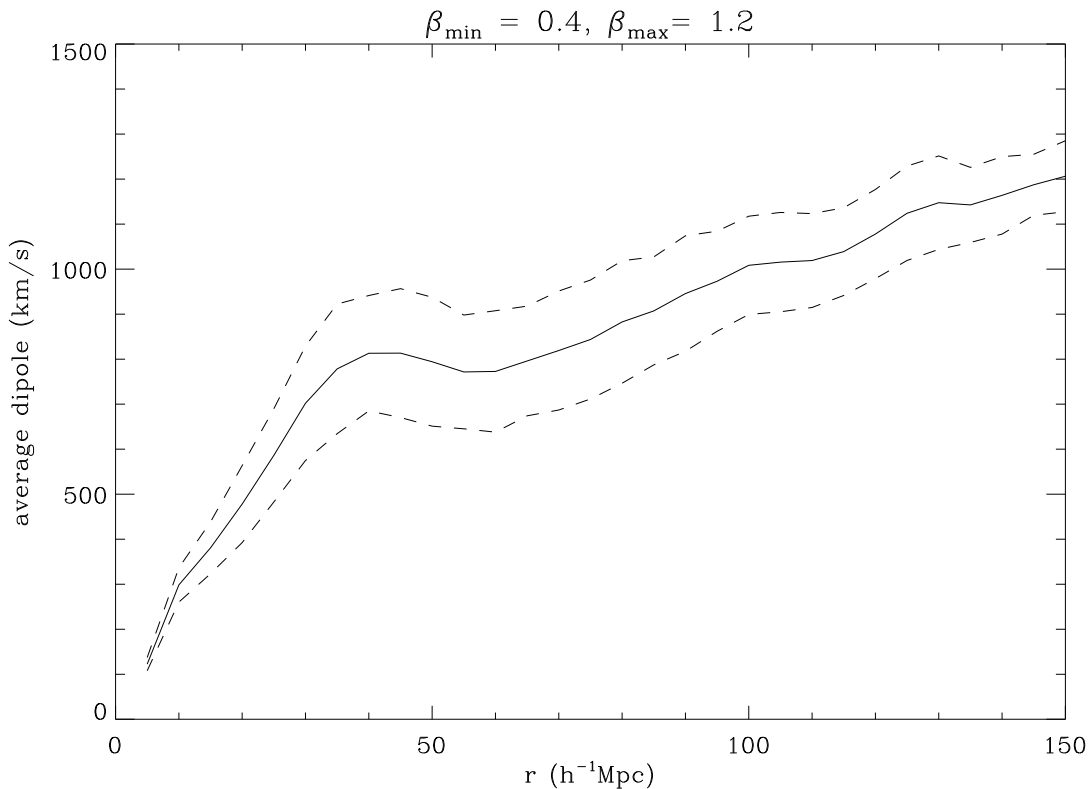


Figure 2. Real Space PSCz cumulative dipole reconstructed with the M1 method using different *a priori* values of β between 0.4 and 1.2. Solid line is the average of all results, dashed lines represent the dipoles calculated with the highest and lowest values for β .

shape of the dipole remains constant at large radii which. This corroborates our previous conclusion that systematic errors induced by the Kaiser rocket effect are far less prominent than in the S92 analysis.

Uncertainties deriving from the nonlinear β scaling will therefore be neglected in the rest of the work.

3.5 The PSCz Dipole

We are now ready to compute the PSCz dipole corrected for systematic biases. Figure 3 shows the magnitude of the cumulative PSCz acceleration up to the limiting depth of $170 h^{-1} \text{Mpc}$, computed after the reconstruction procedure but with no correction for systematic effects. The amplitude is normalised to $\beta = 1.0$. The real space dipole computed using M1 is shown by filled circles while the dipoles from M2 and M3 reconstructions are displayed with squares and open circles, respectively. Error bars representing the same random errors as in figure 1 are displayed for M1 alone to avoid overcrowding. The cumulative dipoles of the three different reconstructions appear to be remarkably similar, despite the very different nature of the techniques used. The same considerations also apply for the dipoles' directions and speak for the reliability of our dipole estimate.

Since the three methods produce equivalent results let us, from now on, concentrate on the M1 dipole only.

Table 1 shows the amplitude of the uncorrected cumulative dipole and the shot noise contribution, both normalised to $\beta = 1$, along with the dipole direction along l and b and the cumulative misalignment angle of the reconstructed PSCz dipole from the CMB dipole apex. The latter quantity is shown in the left panel of figure 4. The misalignment is remarkably small already beyond $40 h^{-1} \text{Mpc}$, i.e. when large overdensities (Great Attractor and Perseus Pisces supercluster) enter the sampled volume. This indicates that contributions to the LG accelerations are coherent over a very large range of scales (Basilakos and Plionis 1998). The right hand panel displays the direction of the cumulative gravity vector measured within $150 h^{-1} \text{Mpc}$ while the error bars quantify the random uncertainties derived from the

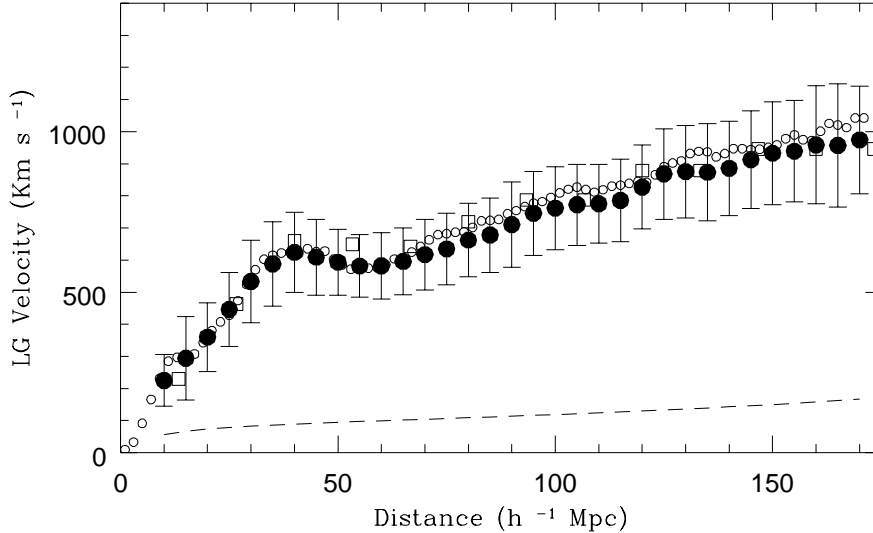


Figure 3. PSCz cumulative acceleration: the amplitude. Black circles represent the amplitude, normalised to $\beta = 1$, of the cumulative PSCz dipole obtained when correcting for redshift space distortions using method 1 (squares = method 2, open circles = method 3). Error bars are the same as in figure 1. The dashed line on the bottom represents the cumulative shot noise error. No correction for systematic uncertainties has been applied.

mocks. The continuous curves are loci of constant misalignment in the (l, b) plane. The asymptotic misalignment angle between LG and CMB dipole $\delta\theta = 15^\circ$ is remarkably small.

Both PSCz and 1.2 Jy samples have been extracted from the same parent PSC IRAS catalogue and have a similar sky coverage. The main difference between the two is the limiting flux which causes the radial selection to be more severe for the IRAS 1.2 Jy galaxies. The dipoles from the two samples should therefore exhibit similar features apart from different shot noise errors. As shown in figure 5, we indeed find a remarkable agreement. The left panel shows the cumulative amplitudes of the two dipoles, both normalised to $\beta = 1$. Filled dots and small triangles refer to the PSCz and 1.2 Jy samples, respectively. Error bars represent random errors for the PSCz dipole alone. Unlike in figure 4, dipoles in figure 5 have been statistically corrected for the systematic errors (as calculated in §3.4), which mainly arise from the rocket effect and the uncertainties in the filling procedure. The two curves on the bottom display the shot noise errors for the PSCz (continuous line) and 1.2 Jy (dashed line). Both corrected dipoles show the same features: a sharp rise followed by a small decrease around $50 h^{-1}$ Mpc as a result of the competing pull of the Great Attractor and Perseus Pisces regions. There is a further slow rise in the PSCz dipole of $\sim 35\%$ in the range

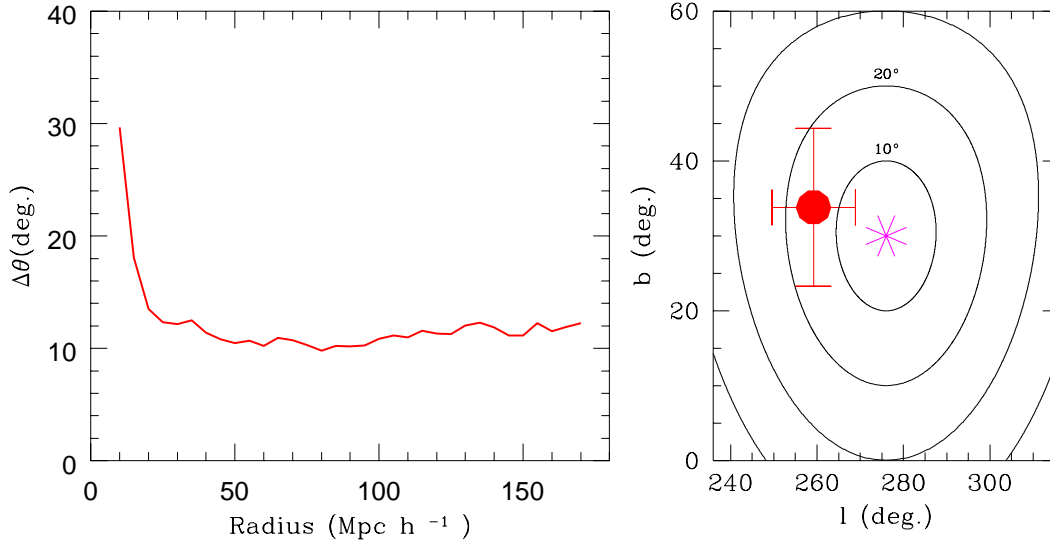


Figure 4. PSCz cumulative acceleration: the direction. The plot on the left shows the cumulative misalignment between PSCz and CMB dipole vectors. On the right the black dot represents the direction on the sky of the cumulative PSC dipole as measured at $150 h^{-1}$ Mpc. Errorbars quantify $1-\sigma$ random errors from the mocks. The starred symbol at the centre shows the CMB dipole directions. Contours are drawn at constant misalignment angles.

between $[60-140] h^{-1}$ Mpc. Both the PSCz and the 1.2 Jy show significant evidence for gravitational contributions beyond $40 h^{-1}$ Mpc. However, unlike the amplitude of the 1.2 Jy dipole, that of the PSCz seems to be constant beyond $\sim 140 h^{-1}$ Mpc. This discrepancy can be accounted for once the different shot noise contributions at large radii are taken into account. The right hand side of figure 5 shows how large the dipole’s misalignment becomes when using the 1.2 Jy catalogue. The 1.2 Jy gravitational acceleration within $150 h^{-1}$ Mpc points $\sim 25^\circ$ away from the CMB dipole, which reduces to a mere $\sim 15^\circ$ when the PSCz sample is considered (see also Kolokotronis *et al.* (1996) who predicted the misalignment of the PSCz dipole to lie between 10 and 17 degrees). Error bars represent random errors – no correction for systematic effects is needed as they mainly affect the dipole’s amplitude.

A further proof of the robustness of our result comes from the comparison with preliminary results from the analysis of the PSCz dipole by Rowan-Robinson *et al.* (1998), which used a different methodology and a much deeper PSCz subsample to address the issue of its convergence. The two dipole estimates agree well within $1-\sigma$ errors. Also note that the above results are fully consistent the recent re-analysis of the 1.2 Jy and QDOT catalogues by Basilakos and Plionis (1998).

R (h^{-1} Mpc)	$ \mathbf{v}_r $ (km s^{-1})	$\sigma_{ \mathbf{v} }$ (km s^{-1})	l (deg.)	b (deg.)	$\Delta\theta$ (deg.)
10	224.8	80.4	252.1	68.7	29.7
20	360.1	107.0	252.0	53.5	13.5
30	533.0	128.8	271.6	42.6	12.2
40	624.0	124.2	269.2	36.9	11.9
50	593.2	102.7	266.9	36.2	10.5
60	582.1	103.2	263.9	30.4	10.2
70	617.0	110.2	263.3	29.7	10.8
80	662.4	114.7	265.1	33.5	9.8
90	710.5	132.4	265.2	36.5	10.2
100	761.5	129.6	262.4	33.7	10.9
110	775.7	122.8	261.3	33.9	10.9
120	827.4	130.7	260.5	34.0	11.3
130	875.5	144.0	257.6	34.5	12.0
140	885.7	147.4	259.4	33.0	11.8
150	932.8	159.6	259.2	33.8	11.1

Table 1. Cumulative PSCz Dipole. Column 1: Distance from the LG in ; Column 2: Cumulative amplitude in ($\beta = 1$); Column 3: Random errors in ($\beta = 1$); Column 4: Cumulative direction along l ; Column 5: Cumulative direction along b ; Column 6: Cumulative misalignment w.r.t. the direction of the CMB dipole.

3.6 A Numerical Estimate of β

In this section, we will evaluate β in a purely numerical way to compare to the likelihood analysis. The idea is similar to that of §3.4, i.e. we use the mock catalogues to evaluate the errors in the reconstructed dipole. Here mock PSCz catalogues are used to statistically correct for the discrepancy between the measured acceleration vector and the true peculiar velocity of an observer. In this exercise we are assuming that the two cosmological models assumed to generate the mock catalogues are realistic. Indeed, the two cosmologies explored produce large scale motions compatible with the observational constraints (Jenkins *et al.* 1998). Moreover, for the cosmological models we have considered, the contribution to the dipole from the wavelength longer than the size of the N-body computational box is small compared to the others errors. Even more so in the inner regions, where a very significant contribution to the LG acceleration comes from. Therefore we do not account for this error source in the present analysis.

For each mock catalogue we compute, at different radii, the ratio between the reconstructed dipole at the observer’s position and its true N-body velocity. The average of the ratios calculated from the various mock catalogues provides us with a multiplicative factor which relates the dipole reconstructed by our method to the real LG velocity. We calculate this for all three Cartesian components and find that the multiplicative factors are sufficiently similar to warrant averaging.

Note that, unlike in §3.4, the discrepancy between reconstructed dipole and real velocity is caused by the effects of non-linearity, shot noise, finite volume and residual redshift space distortions i.e. this now represents the cumulative effect of *all* sources of error. Note also that the multiplicative factor and its dispersion do not depend on β in the first approximation when it has been averaged over all catalogues. The reconstructed dipoles have been scaled to what is in each case known to be the correct β of the simulation so that the ratio between the reconstructed and the real dipole velocity only depends on the various errors and not on cosmology.

We then use this multiplicative factor to recover the LG peculiar velocity from the reconstructed cumulative PSCz dipole to be compared with CMB dipole, v_c , to evaluate β .

Figure 6 shows the result of this procedure. Surprisingly, β is remarkably stable around 0.7 even at low radii, where the volume includes little of the mass distribution that really causes the total LG acceleration. However, the errorbars on those scales are correspondingly larger. The errors, which represent the dispersion in the distribution of cumulative factors obtained from the mocks, are asymmetric, which indicates that it will be easier to set a lower rather than an upper limit on β .

The dashed and two dotted lines show the result of the likelihood analysis performed in §4.3 (figure 7a and 7b).

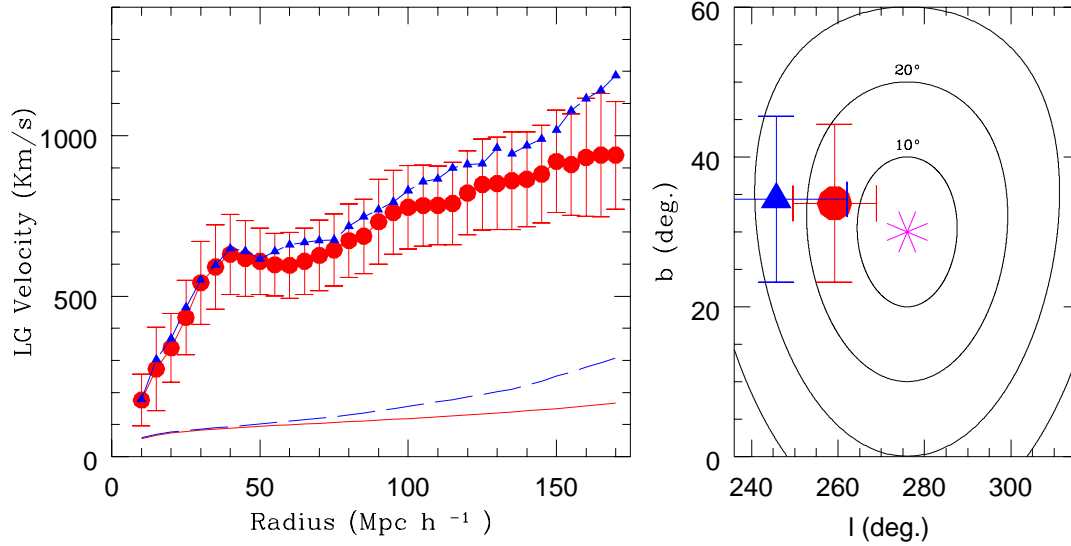


Figure 5. PSCz vs. 1.2 Jy dipoles. The amplitudes of the PSCz and the 1.2 Jy dipoles, both corrected for systematic errors, are shown in the left plot using filled dots and triangles, respectively. Error bars represent $1-\sigma$ uncertainties. The lines on the bottom indicate the cumulative shot noise error for the PSCz dipole (continuous line) and for the 1.2 Jy one (dashed line). On the right plot the same symbols indicate the directions of the two dipoles at $150 h^{-1}$ Mpc.

The dashed line represents the most likely β -value, the dotted lines the β $1 - \sigma$ range. It is encouraging that the numerical analysis is entirely consistent with the likelihood analysis.

4 LIKELIHOOD ANALYSIS

4.1 Velocity Statistics

Our aim is to assess the likelihood of a given cosmological model using all the information we have on velocities in the local universe, i.e. the measured LG velocity, the CMB dipole, the bulk velocity, and the LG velocity residual. To this end, we need to find a mathematical expression for the probability distribution functions (joint or constrained) of the velocities available and the first step is to find expressions for these velocities. In the present analysis, which is based on the work of Juszkiewicz, Vittorio and Wise (1990) and S92, all velocities are regarded as Gaussian random vectors.

In the limit of a finite survey volume, the peculiar velocity of the Local Group becomes

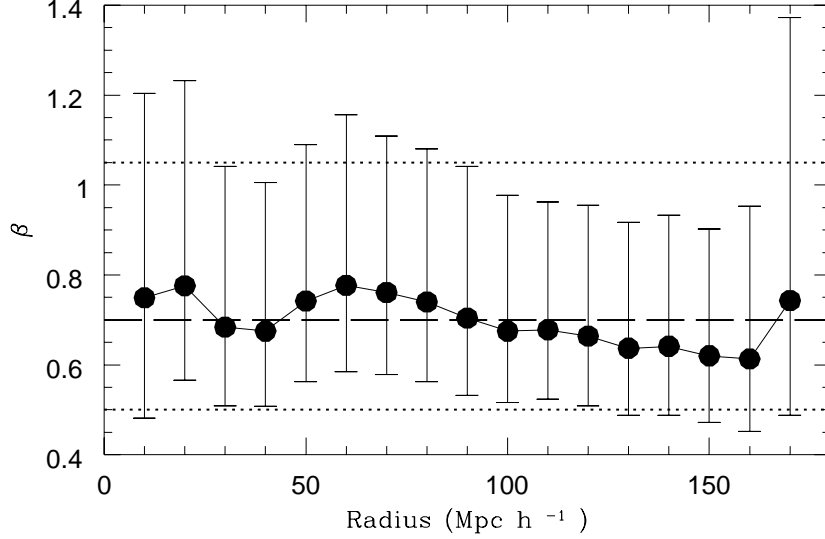


Figure 6. Robustness Test. Filled dots represent the β value obtained when comparing the LG velocity deduced from the CMB dipole to the one numerically deduced from the PSCz acceleration. Errorbars represent 1- σ uncertainties estimated from the mock PSCz catalogs. The dotted and the dashed lines represent the 1- σ level range for the value of beta from the likelihood analysis ($\beta = 0.7^{+0.5}_{-0.2}$).

$$\mathbf{v}_i = \frac{H_o\beta}{4\pi} \int d^3\mathbf{r}' W_i(r) \frac{\mathbf{r}'}{|\mathbf{r}'|^3} \delta_g(\mathbf{r}') \quad (6)$$

where the window function $W_i(r)$ specifies the finite survey volume. It is often more convenient to work in Fourier space in which case eqn. (6) becomes

$$\mathbf{v}_i = H_o\beta \int d^3\mathbf{k} \tilde{W}_i(k) \frac{i\mathbf{k}}{(2\pi)^3 k^2} \delta_g(\mathbf{k}), \quad (7)$$

where \mathbf{k} is the wavenumber vector, $\tilde{W}_i(k) = k \int dr W_i(r) j_1(kr)$, is the window function in Fourier space and $j_1(kr)$ is the spherical Bessel function of order 1. This expression represents the linear velocity of the LG that is expected to be measured through a given window function in a universe characterised by the density field δ_g . To make use of the information stored in the growth of the cumulative LG acceleration vector with radius of the sampled volume, we will find it more convenient to measure the differential LG velocity, $\mathbf{v}_{r,i}$ generated within a series of N non-overlapping top-hat window functions between radii r_i and r_{i+1} ,

$$\tilde{W}_i(k) = \frac{\sin(kr_i)}{kr_i} - \frac{\sin(kr_{i+1})}{kr_{i+1}} \quad (8)$$

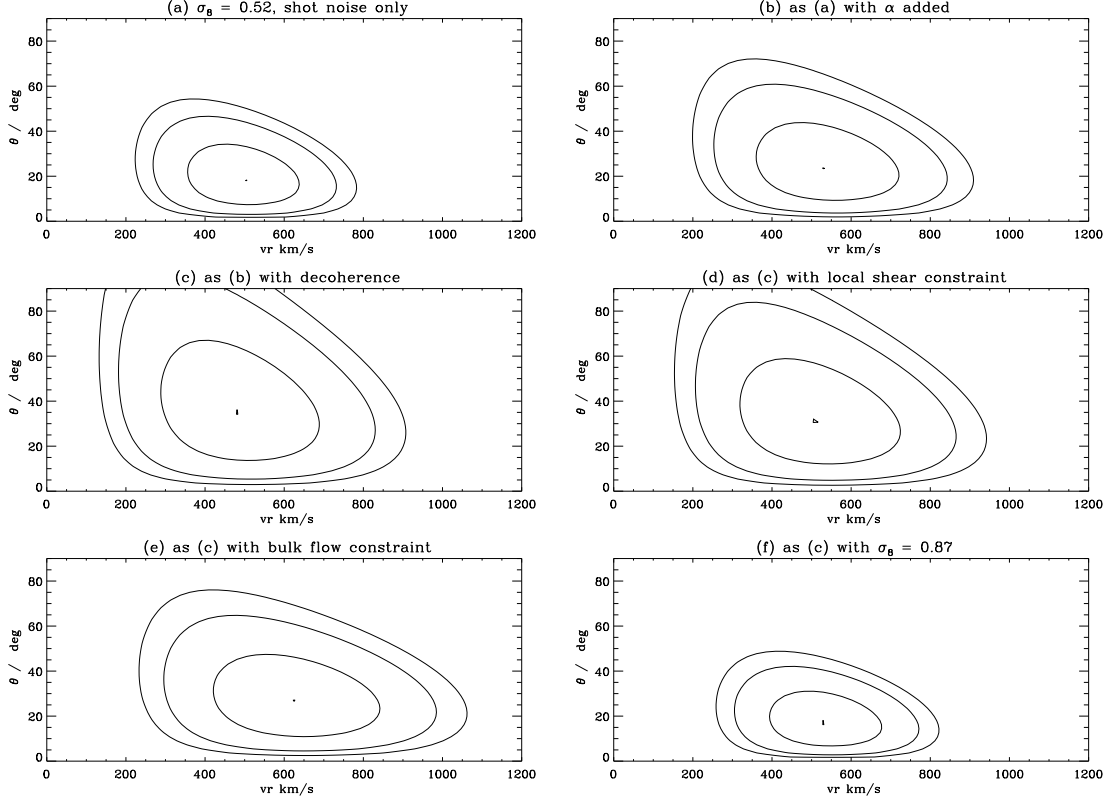


Figure 7. Probability of Amplitude and Misalignment. Likelihood contours for amplitude and misalignment of the PSCz dipole in a specified world model. Fig 7a refers to the case of ($\Gamma = 0.5, \beta = 1, \sigma_8 = 0.52$) universe while contours refer to $\mathcal{L}(\mathbf{v}_r | \mathbf{v}_{CMB})$. Fig 7b show the effect of introducing the reconstruction errors, α , and Fig 7c also includes the decoherence effects. Fig 7d and e show the effect of introducing either the shear or the bulk flow constraints, respectively. Figure 7f show the same case as figure 7d for a ($\Gamma = 0.195, \beta = 0.55$ and $\sigma_8 = 0.87$) model.

with $i = 2, \dots, N$. In the innermost region ($i = 1$) we smooth with a top hat filter on scales smaller than $r_s = 5 h^{-1} \text{Mpc}$ to eliminate strong nonlinear effects. Therefore, the window function for the innermost region is of the form

$$\tilde{W}_1(k) = \frac{3j_1(kr_s)}{kr_s} - j_0(kr_1). \quad (9)$$

The total measured LG velocity \mathbf{v}_r can be obtained when $N = 1$ and $r_1 = R_{max}$ is the sample's depth.

The other velocities modelled in this analysis are equally characterised by different window functions. The $N+1$ th velocity vector considered is the true LG velocity measured in the CMB frame, \mathbf{v}_c . Its window function extends over all space except for a small-scale cut-off to account for the finite size of the Local Group. In k -space its form is

$$\tilde{W}_{CMB} = \frac{\sin(kr_{LG})}{(kr_{LG})}, \quad (10)$$

where $r_{LG} = 1 h^{-1} \text{Mpc}$.

The velocity field within the neighbourhood of the Local Group is remarkably quiet (*cf.* Peebles 1998). The observed LG velocity residuals \mathbf{v}_s , i.e. the difference between the Local Group velocity and the average velocity within a sphere of $5 h^{-1} \text{Mpc}$, is less than 200 km s^{-1} . This can be used as an effective constraint in a likelihood analysis of the LG dipole field and we take the amplitude of the velocity residuals as the $N + 2$ th random variable. The window function for the LG velocity residuals within $r_a = 5 h^{-1} \text{Mpc}$ is

$$\tilde{W}_s(k) = 1 - 3 \frac{\sin(kr_a) - kr_a \cos(kr_a)}{(kr_a)^3}. \quad (11)$$

The final $N + 3$ th random vector we consider is the bulk velocity \mathbf{v}_b measured within $r_b = 30 h^{-1} \text{Mpc}$ from the POTENT analysis of the Mark III catalogue of galaxy peculiar velocities (Dekel 1997). Since we consider POTENT-processed data the measured bulk velocity is just the average peculiar velocity of a spherical region of $30 h^{-1} \text{Mpc}$. This allows us to express the relative window function for the bulk flow as

$$\tilde{W}_b(k) = 3 \frac{\sin(kr_b) - kr_b \cos(kr_b)}{(kr_b)^3}. \quad (12)$$

Since we model all the $N + 3$ velocities as Gaussian random vectors, any probability distribution function will only depend on the covariance matrix:

$$\begin{aligned} M_{lm} &= \frac{1}{3} \langle \mathbf{v}_l \cdot \mathbf{v}_m \rangle \\ &= \frac{H_0^2 \beta^2}{6\pi^2} \int dk P(k) \tilde{W}_l(k) \tilde{W}_m(k), \end{aligned} \quad (13)$$

where $P(k) = \langle \delta(k) \delta(k) \rangle$ is the power spectrum of density fluctuations and $\tilde{W}_l(k)$, $\tilde{W}_m(k)$ are any of the window functions that we have previously introduced. In this paper, we restrict our analysis to the family of CDM power spectra for which we use the expression of Davis *et al.* (1985), characterised by the shape factor $\Gamma = \Omega_m h$:

$$P(k) = \frac{Bk \exp[-\frac{1}{2}(kg_s)^2]}{[1 + 1.7k/\Gamma + 9(k/\Gamma)^{3/2} + (k/\Gamma)^2]^2} \quad (14)$$

where $g_s = 100 \text{ km s}^{-1}$ and the only function of the exponential term is to improve numerical stability. h is the Hubble constant in units of $100 \text{ km s}^{-1} \text{ Mpc}^{-1}$ and B is the normalisation constant. As anticipated in §3.3, we normalise the power spectrum to σ_8 according to the Eke, Cole and Frenk (1996) prescription. Thus, we can completely characterise the CDM background cosmology by specifying β , Γ and Ω_Λ .

4.2 Probability Distributions

The Gaussianity of the velocity field guarantees that the joint distribution function of all our N+3 model velocities is also a multivariate Gaussian:

$$f(\mathbf{v}_r(i), i = 1..N, \mathbf{v}_c, \mathbf{v}_s, \mathbf{v}_b) = (2\pi)^{-3(N+3)/2} (\det M)^{-3/2} \exp(-\frac{1}{2} \mathbf{v}_l \cdot \mathbf{v}_m (M^{-1})_{lm}) d\mathbf{v}_r d\mathbf{v}_c d\mathbf{v}_s d\mathbf{v}_b \quad (15)$$

where l, m take values from 1 .. N+3 and Einstein summation convention is assumed. This represents the relative probability of observing any given set of these velocities in some assumed CDM universe specified by (β, Γ) and the normalisation σ_8 . To treat any of \mathbf{v}_c , \mathbf{v}_b , or \mathbf{v}_s as a constraint, we have to calculate the ratio of the joint probability to the probability of the constraint. For example, the probability distribution function of $f(v_r(i), i = 1..N | v_c)$ is given by

$$f(v_r(i), i = 1..N | v_c) = (2\pi)^{-3N/2} \left(\frac{M_{cc}}{\det M} \right) \exp \left[-1/2 \left(\mathbf{v}_l \cdot \mathbf{v}_m (M^{-1})_{lm} - \frac{v_c^2}{M_{cc}} \right) \right] d\mathbf{v}_r(i) \quad (16)$$

Any other constraint is similarly easy to express. For the CMB dipole vector we use the recent determination by Lineweaver *et al.* (1996) quoted in the introduction. For the bulk flow vector we use the Mark III-POTENT estimate at $R_b = 30 h^{-1} \text{ Mpc}$ ($437 \text{ km s}^{-1} \pm 40 \text{ km s}^{-1}$, $l=306^\circ$, $b=14^\circ$ Dekel 1997). We have chosen not to use the Mark III-POTENT at large radii, which would set a more stringent constraint, because of the problems in the calibration of the distance indicators recently discussed by Willick and Strauss (1998) beyond $30 h^{-1} \text{ Mpc}$. Within a scale of $30 h^{-1} \text{ Mpc}$, however, Mark III velocities have proved to be reliably calibrated and fully consistent with the 1.2 Jy gravity field (Willick *et al.* 1997 Davis, Nusser and Willick 1996).

For the LG velocity residuals, we impose a constraint on their magnitude $v_s \leq 200 \text{ km s}^{-1}$, which means that the appropriate probability distribution has to be integrated over a sphere of radius $v_a = 200 \text{ km s}^{-1}$. The expressions for the various conditional distribution functions involving the first $N + 2$ vectors, $f(\mathbf{v}_r(i) | \text{constraints})$, have all been derived by S92, and can be easily extended to include the bulk velocity vector.

By construction, the various probability distributions already account for errors arising from the use of finite window functions. However, as we have already pointed out, there are other error sources that we need to account for explicitly:

- As mentioned above, we adopt the shot noise definition of S92 (their eq. (35)) which accounts for sparse sampling as well as the unknown mass function of the IRAS galaxies. The latter is quantified by the mass variance which for PSCz galaxies, in the S92 formalism, is $K = 1$. As displayed in figure 3, the PSCz shot noise increases with radius.

We calculate the shot noise contribution to the differential dipole in each shell, square it and add it to the diagonal elements of the covariance matrix, M_{ii} , with $i \leq N$.

- The PSCz dipole is measured from the real space position of galaxies which we obtain after minimising the redshift space distortions iteratively. Intrinsic errors in the reconstruction procedure generate an average random error of 15 km s^{-1} in the differential dipole (*cf.* §3.4) produced by a shell of matter $10 h^{-1} \text{ Mpc}$ wide. This error, α , is added in quadrature to the first $i = 1 \dots N$ diagonal elements of the covariance matrix just like the shot noise.

- Nonlinear motions spoil the alignment between \mathbf{v}_r and \mathbf{v}_c . To account for these effects, we follow S92 and define a decoherence function in k -space which expresses the misalignment between the Fourier components of the LG velocity $\mathbf{v}_{r,k}$ and the CMB dipole $\mathbf{v}_{c,k}$:

$$W_d(k) = \frac{\langle \mathbf{v}_{r,k} \cdot \mathbf{v}_{c,k} \rangle}{|\mathbf{v}_{r,k}| |\mathbf{v}_{c,k}|}. \quad (17)$$

This additional window function multiplies the integrands that describe the covariance between measured accelerations and LG velocity, i.e. the terms M_{ij} with $i \leq N$, $j = N + 1$ and their conjugates. Clearly, since nonlinear effects are more severe on small scales, $W_d(k) \rightarrow 0$ at large k . To model $W_d(k)$ we use the S92 expression

$$W_d(k) = \frac{1}{(1 + (kr_d)^4)^{\frac{1}{2}}}. \quad (18)$$

We put the decoherence length $r_d = 4.5 h^{-1} \text{ Mpc}$ which S92 templated using N-body simulation of a standard CDM cosmology. In adopting this expression we follow the S92 assumption that the decoherence function does not change appreciably with the background cosmology.

From the probability density distributions introduced above and the measured PSCz dipole, it is possible to evaluate the relative likelihood, \mathcal{L} , of different world models $(\beta, \Gamma, \sigma_8)$. We define the likelihood function as

$$\mathcal{L} = -2 \ln(f), \quad (19)$$

which is conveniently distributed like χ^2 around its minimum. In the next two sections we will perform two different likelihood analyses with the aim of constraining the β and Γ parameters that, along with σ_8 , specify the underlying cosmological model.

4.3 Probability of Amplitude and Misalignment

The aim of this first section is to afford us some insight into what kind of dipole we are likely to measure given a model of the universe and certain constraints. We do this by measuring the probability that an LG-like observer carrying out a PSCz-like survey measures a velocity \mathbf{v}_r in a given $(\beta, \Gamma, \sigma_8)$ universe. We characterize the LG velocity by its amplitude measured within a specified window, v_r , and the misalignment to the CMB dipole θ . Since we want to plot the values of the likelihood distribution only as a function of v_r and θ , we compute the constrained probability rather than the joint one. It is worth noting that v_r scales with the assumed β and that the differential element in the probability distribution becomes $d\mathbf{v}_r = \beta^3 v_r^2 \sin(\theta) dv_r d\theta d\phi$.

Figure 7 shows 68 %, 90 %, and 95 % likelihood contours from six probability distributions. In all cases the acceleration is measured within the same spherical window function of radius $150 h^{-1} \text{ Mpc}$ which means that we will be using the window function of eqn. (9) in which $R_{max} = 150 h^{-1} \text{ Mpc}$. In figure 7a we plot $\mathcal{L}(\mathbf{v}_r | \mathbf{v}_c)$ for a universe with $\Gamma = 0.5$, $\beta = 1$ and $\sigma_8 = 0.52$, only accounting for shot noise errors (it can be shown that in the absence of shot noise and with an infinitely deep window function the likelihood contours reduce to a point around $\theta = 0$ and $v_r = 620 \text{ km s}^{-1}$). The variance in the predicted direction and amplitude (i.e. the width of the contour lines) is remarkable which shows how misleading it can be to evaluate β from a direct comparison between v_r and v_c . It becomes slightly larger when accounting for the errors in the reconstruction procedure, α , as shown in figure 7b. The inclusion of the decoherence has an even more dramatic effect on the likelihood contours. Figure 7c shows how seriously our ignorance in modelling nonlinear motions can affect the determination of the true dipole. The effect of decoherence is to eliminate the large k -modes which greatly increases the variance in the measured dipole direction

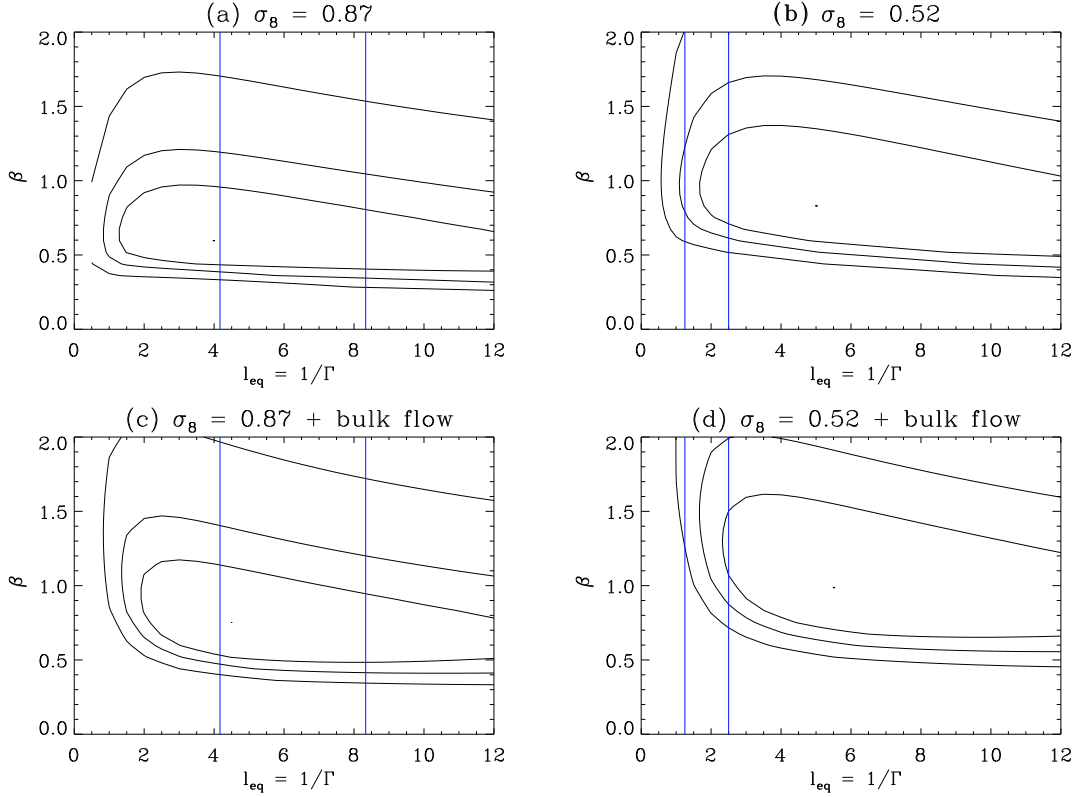


Figure 8. Probability of (β, Γ) . The plots 8a and 8b show the likelihood contours of $\mathcal{L}(\mathbf{v}_r(i), i = 1, 15, \mathbf{v}_c | v_s < v_a)$, while the bulk flow constraint is introduced in figures 8c and 8d. The case for a high normalisation ($\sigma_8 = 0.87$) is shown in figures a and c. A smaller value of $\sigma_8 = 0.52$ is used to normalise the model plotted in figures b and d. Vertical dashed lines delimitate the range in which $0.4 < h < 0.8$ as suggested by observations. They have been drawn assuming that the normalisation is meant to reproduce the cluster abundance.

and brings the most likely misalignment up to $\sim 30^\circ$. The LG velocity residuals constraint imposes an upper limit on the amplitude of nonlinear contributions to peculiar velocities that originate on small scales and thus should reduce the variance introduced by the decoherence. As shown figure 7d, however, the effect on the likelihood contours is quite minor. Much better results are obtained when including the bulk flow constraint, as is shown in figure 7e where we have replaced the velocity residuals constraint with the bulk flow one. The variance in θ is greatly reduced and the peak of the likelihood moves towards larger values of v_r . This behaviour derives from imposing that \mathbf{v}_r and \mathbf{v}_c be well aligned which, together with the CMB dipole amplitude constraint, forces a significant part of the LG acceleration to originate within $30 h^{-1}\text{Mpc}$.

Finally, in figure 7f we have changed the background cosmology $(\beta, \Gamma, \sigma_8)$. The plot shows the same case as figure 7c but refers to a $\sigma_8 = 0.87$ normalization with $\Gamma = 0.195$ and $\beta = 0.55$. This model has smaller power on small scales, which considerably reduces the spread of the likelihood contours. The position of the central peak, however, does not change appreciably. This reflects the fact that CDM models normalised to the cluster abundance produce large scale motions with similar properties (Jenkins *et al.* 1997). In particular the most likely velocity of a LG-like observer remains remarkably constant.

4.4 Probability of (β, Γ)

In the second part of this analysis, we consider a series of different (β, Γ) universes and compute, for each of them, the likelihood of obtaining the same dipole as measured from the PSCz subsample within a specified window function and for a fixed σ_8 normalisation. The likelihood contours can then be displayed in a two-dimensional (β, Γ) plane. Note that the Eke, Cole and Frenk (1996) normalisation allows one to relate σ_8 to Ω_m , which defines a $(\beta, \Gamma) \rightarrow$

(b, h) transformation. In the following, we will, however, normally disregard this transformation and consider the normalisation simply as a fixed parameter. Also, allowing for a non-vanishing cosmological constant does not change the overall picture, as we have tested by comparing figure 8a with analogous contours produced for an $\Omega_m = 0.3$, $\Omega_\Lambda = 0.7$ scenario. We therefore limit our discussion to the case of a $\Omega_\Lambda = 0$ universe.

Figure 8 shows likelihood contours of $\beta, l_{eq} = 1/\Gamma$ for two different choices of σ_8 (we have chosen to use the parameter l_{eq} to allow easier comparison of our results to those of S92). Confidence levels in this case are 68, 90, 99 %, which translates into $\Delta\mathcal{L}$ of 2.3, 4.6, and 9.2 since there are 2 degrees of freedom in the distribution. The function plotted is $\mathcal{L}(\mathbf{v}_r(i), i = 1 \dots N, \mathbf{v}_c | v_s < v_a)$ in which we use $N = 15$ non-overlapping top-hat windows of width $10 h^{-1}$ Mpc. This makes use of the data we have on the growth rate of the dipole up to a distance of $150 h^{-1}$ Mpc, as plotted in figure 5.

Figure 8a,b show confidence contours of the function for both normalisations ($\sigma_8 = 0.87$ and $\sigma_8 = 0.52$ respectively). Shot noise, intrinsic reconstruction errors, α , and decoherence effects are all taken into account. Note that with respect to the analysis of the IRAS 1.9Jy dipole by S92 (*cf.* their figures 13 and 14) our constraints on Γ are somewhat weaker. This difference arises in part from the fact that, as we have pointed out, the PSCz dipole receives non-negligible contribution from mass inhomogeneities beyond $40 h^{-1}$ Mpc, implying that models with large power (large l_{eq}) cannot easily be ruled out, whereas the data used by S92 does not indicate any appreciable increase beyond $40 h^{-1}$ Mpc. The two different contours in figures 8a and 8b have basically the same shape, which indicates that the analysis is not overly sensitive to the normalisation of the power spectrum. Both exclude very small β (< 0.4) at the highest confidence level. This is not surprising since a very small β would not be able to produce the measured velocities. The range of allowed β is larger in the low-normalisation case and slightly shifted towards higher values because small fluctuations in the density contrast can only cause the observed velocities when coupled with higher masses. In neither case can we make any restrictive statement about Γ , except that the power cannot be confined to the very smallest scales. The peak of the likelihood distribution is shifted towards slightly higher powers in figure 8b, again because if the fluctuations are small and the density is generally larger, then power on large scales is more likely to be responsible for the observed velocities. The peak of the likelihood distribution in both cases is roughly consistent with the $\Gamma \simeq 0.2$ measured by Tadros & Efstathiou (1995) from the IRAS survey.

As mentioned above, the normalisation can be regarded as a constraint on Ω_m ($\Omega_m = 0.3$ for case 8a and $\Omega_m = 1.0$ for 8b). In that case, the β - transforms to a b -axis and the Γ - to a h -axis. In figures 8a,b the vertical lines indicate the range of currently accepted h ($[0.4;0.8]$), thereby indicating an extra constraint on Γ if Ω_m is considered fixed. In both cases, this additional constraint is consistent with the likelihood contours. In case 8b, however, it only allows fairly high values of Γ , i.e. the high Ω_m (coupled with a low normalisation to reproduce the observed cluster abundance) and a value of h in the given range force the power to originate on much smaller scales than seems most likely from the measured velocities (or indeed than was measured from the IRAS survey as mentioned above).

Figures 8c and 8d show the effect of including the bulk flow constraint in figures 8a and 8b, respectively. The bulk velocity is mainly determined by the shape and the amplitude of the power spectrum on large scales. It is not surprising, therefore, that imposing the Mark III–POTENT bulk velocity constraint tends to favour cosmological models with excess power on large scales. Since the bulk flow is well aligned with the dipole, it also excludes the combination of low β and high Γ in both normalisations. In both cases, if the power is on small scales, the observed bulk flow can only be generated with a very high β . However, in figures 8c,d as well as in 8a,b, the likelihood analysis cannot set stringent limits on the shape parameter. We only find that $\Gamma < 0.4$ in case of low normalisation and that $\Gamma < 0.5$ for the high-normalisation case. Both limits refer to the 68 % confidence limit level.

The likelihood analysis allows determination of β with much better accuracy than Γ . In the high-normalisation case we obtain $\beta = 0.7_{-0.2}^{+0.5}$ with 68% confidence. Note that this is the range allowed by the likelihood contours in figure 8. We can tighten these constraints by marginalising over the values of Γ allowed by the h -constraints. This yields $\beta = 0.7_{-0.2}^{+0.35}$ (see figure 9 for the marginalised probabilities corresponding to figure 8). The resulting bias parameter for IRAS galaxies is $b = 1.43_{-0.2}^{+0.35}$, in accordance with the range of the values allowed by independent

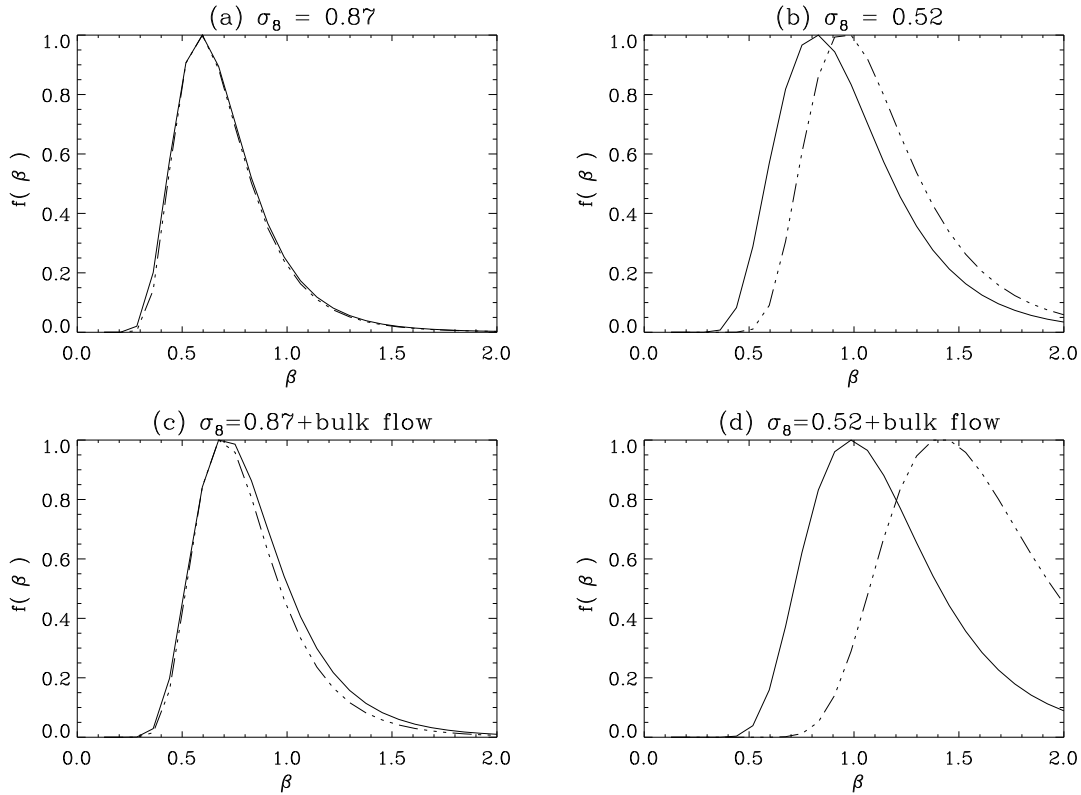


Figure 9. Marginalised likelihood distribution. Marginal distribution of the likelihood of β obtained from likelihood distribution. Plots a,b,c and d refer to their analogous cases in figure 8. Continuous lines show the result of integrating over all the values of Γ . Dot dashed lines are obtained when limiting the integration range between the vertical dashed lines displayed in figure 8.

observations and analyses. With $\sigma_8 = 0.52$ the likelihood contours shift upwards, increasing the most likely β value to $1.0^{+0.6}_{-0.3}$ again at 68% confidence level.

5 CONCLUSIONS

We have measured the LG acceleration vector using the IRAS PSCz galaxy distribution in real space. Three independent methods have been used to correct for redshift space distortions and to keep systematic reconstruction errors under control. As pointed out by S92, apart from the shot noise, the Kaiser rocket effect represents the most serious uncertainty in the dipole measurement. In this work we have accounted for this and all the other sources of systematic errors by using PSCz mock catalogues from N-body simulations.

The resulting PSCz acceleration vector appears to receive a non-negligible contribution from scales larger than $40 h^{-1}$ Mpc, unlike in the IRAS 1.9 Jy (S92) and ORS (Strauss 1996) analyses. We find that between 60 and $140 h^{-1}$ Mpc the dipole amplitude increases by $\sim 35\%$ and that only beyond this scale we find evidence for convergence. This result is in agreement with the recent analysis by Rowan-Robinson *et al.* (1998) and also confirms the reality of the large-scale contributions to the LG accelerations advocated by Scaramella *et al.* (1991), Plionis & Valdarnini (1991) and Branchini & Plionis (1996) on the basis of the distribution of the Abell-ACO clusters. The misalignment of the measured with the CMB dipole is remarkably small ($\sim 15^\circ$) and stays almost constant beyond $40 h^{-1}$ Mpc which corroborates the impression that most of the LG acceleration is generated from density fluctuations along the Perseus Pisces-Great Attractor-Shapley concentration baseline. The IRAS 1.2 Jy dipole appears to be fully consistent with the PSCz if the shot noise contribution is properly accounted for. The increasing importance of shot noise and rocket effect beyond the depth of our mock catalogues leads us to limit our PSCz dipole analysis to within $170 h^{-1}$ Mpc.

The measured PSCz cumulative dipole has been fed into a likelihood analysis with the aim of constraining the β

parameter and the shape factor, Γ , assuming a CDM framework and a given normalisation for the power spectrum. The formalism accounts for shot noise errors, finite window size, nonlinear effects and random uncertainties introduced when minimising redshift space distortions. To better determine β and Γ , observational constraints on the LG velocity residuals, bulk flow, and LG velocity relative to the CMB frame have been introduced in the analysis. We account for the freedom in the spectrum normalisation by exploring two different cases: $\sigma_8 = 0.52$ and $\sigma_8 = 0.87$. In both scenarios we find that the PSCz dipole does not allow to set stringent limits on the shape parameter Γ . However, if the normalisation is intended to reproduce the observed cluster abundance, then a relation between σ_8 and Ω_m results and further limits on Γ can be set by constraining the Hubble constant within the range allowed by observations. As a result we find that in a critical universe (i.e. for $\sigma_8 = 0.52$), Γ is constrained to be between 0.4 and 1.0 which is well outside the range of recent Γ estimates, like the one coming from power spectrum analyses of the IRAS survey (Tadros & Efstathiou 1995) for which $\Gamma \simeq 0.2$. It should however be noted that the introduction of the constraints on h implies that $\Gamma = \Omega_m h$, and will not hold for more general expressions of the shape parameter.

The likelihood analysis produces more stringent constraints on the β value. For the high normalisation case (figure 8a) we find that $\beta = 0.70^{+0.3}_{-0.2}$ at $1-\sigma$ level. A result that does not change when the bulk flow constrain is introduced (figure 8c). These results indicate that, if cluster normalisation is assumed, then a low density universe is very much consistent with observations and allows determination of the β parameter with $\sim 35\%$ accuracy .

When adopting a low normalisation, the constraints over β change appreciably with those on h and on the bulk flow. In particular, they change drastically with h when considering a low normalisation together with the bulk flow. The low normalisation implies that β has to be very high ($\beta \simeq 1.5$) to produce the measured bulk flow (if h is fixed within the given bounds). This is much higher than β determined from other dynamical measurements. Together with the fact that the range in h also forces Γ to be much higher than indicated by independent measurements, this implies that the model is probably not realistic.

Our ability in determining β from the galaxy dipole is mainly hampered by our ignorance of the large scale contribution to the LG acceleration by the fact that the likelihood analysis is based on one single observer. Better determinations of β have been obtained by comparing MarkIII POTENT measured velocities to the ones modelled from the 1.2 Jy catalog (Davis, Nusser and Willick, Willick et. al 1997, Willick and Strauss 1998, da Costa, Nusser et al 1998). A substantial improvement, however, can only be obtained by comparing the PSCz gravity field with observed velocities at many independent locations. An analysis of this kind using the recent SFI data (Giovanelli *et al.* 1997a, 1997b) is currently in progress.

ACKNOWLEDGMENTS

This work was supported by various PPARC grants and by the EC TMR network for research in ‘‘Galaxy formation and evolution.’’ CSF acknowledges a PPARC Senior Research Fellowship. LFAT was supported by the PRAXIX XXI programme of JNICT (Portugal). IS and EB thank Michael Strauss for many useful comments and suggestions.

REFERENCES

- Basilakos, S. and Plionis, M. 1998, MNRAS, 299,637
- Branchini, E., Plionis, M., 1996, ApJ, 460, 569
- Branchini, E., Teodoro, L., Frenk, C. S., Schmoldt, I., Efstathiou, G., White, S.D.M., Saunders, W., Sutherland, S., Rowan-Robinson, M., Tadros, H., Maddox, S and Oliver, S., 1998 MNRAS *submitted*
- Brown, M., and Peebles P. 1987, ApJ 317, 588
- Cole, S., Hatton, S., Weinberg, D., and Frenk C. 1998, MNRAS, 300, 945
- da Costa, L., Nusser, A. et al 1998, MNRAS, 299, 425
- Davis, M., Efstathiou, G., White, S., and Frenk, C. 1985, ApJ 292,371
- Davis M., Nusser, A., Willick J. 1997, ApJ 473, 22
- Dekel, A, 1997, in da Costa L.N., Renzini A., eds, Galaxy Scaling Relations. Springer, p. 245
- Eke, V., Cole, S., and Frenk, C. 1996, MNRAS 282,263
- Fisher, K., Huchra, J.P., Strauss, M., Davis, M., Yahil, A., Schlegel, D. 1995, ApJS, 100, 69.
- Giovanelli R., Haynes M., Herter T., Vogt N., Wegner G., Salzer J., da Costa L., Freudling W., 1997a, AJ, 113, 22
- Giovanelli R., Haynes M., Herter T., Vogt N., da Costa L., Freudling W., Salzer J., Wegner G., 1997b, AJ, 113, 53
- Guzzo, L., Strauss, M., Fisher K., Giovanelli, R., and Haynes M. 1997, ApJ, 489, 37
- Kolokotronis, V., Plionis, M., Coles, C., and Borgani, S. 1996, MNRAS 280,186
- Jenkins. A., et al. (The Virgo Consortium) 1998, ApJ, 499, 20
- Kaiser, N. 1987, MNRAS, 227,1
- Kaiser N., and Lahav, O., 1988, in Rubin V.C., Coyne G., eds, Large Scale Motions in the Universe: A Vatican Study Week. Princeton Univ. Press, Princeton, p. 339
- Lineweaver, C.H., Tenorio, L., Smoot, G.F., Keegstra, P., Banday, A. J., and Lubin, P. 1996, ApJ 470,38L
- Nusser, A., and Davis, M. 1994, ApJ, 421, 1L
- Paczynski, B., and Piran, T. 1990, ApJ, 364, 341
- Peebles P.J.E., 1980, The Large Scale Structure of the Universe, Princeton University Press, Princeton
- Peebles P.J.E., 1998, ApJ 332,17
- Plionis M., and Valdarmini R., 1991, MNRAS, 249, 46
- Plionis M., and Kolokotronis, V., 1998, ApJ, 500,1
- Rowan-Robinson M., Lawrence A., Saunders W., Crawford J., Ellis R., Frenk C.S., Parry I., Xiaoyang X., Allington-Smith, J., Efstathiou G., Kaiser N., 1990, MNRAS, 247, 1
- Rowan-Robinson M *et al.* 1998 *in preparation*
- Santiago, B. X., Strauss, M., Lahav, O., Dressler, A., and Huchra, J., 1995, ApJ, 446, 457
- Santiago, B. X., Strauss, M., Lahav, O., Davis, M., Dressler, A., and Huchra, J., 1996, ApJ, 461, 38
- Scaramella R., Vettolani G., Zamorani G., 1991, ApJ, 376, L1
- Strauss M.A., Ostriker, J., and Cen, R. 1998, ApJ, 493,39.
- Strauss M.A., Willick J.A., 1995, Phys Rep., 261, 271
- Strauss, M., 1997, in N. Turok ed., Critical Dialogues in Cosmology, World Scientific, p.423.
- Strauss M.A., Yahil A., Davis M., Huchra J.P., and Fisher K., 1992, ApJ, 397, 395 [S92]
- Tadros, H., Efstathiou, G. 1995, MNRAS, 276,L45
- Willick, J., Strauss, M., Dekel, A., and Kolatt, T. 1997, ApJ, 486, 629
- Willick, J., and Strauss, M. 1998, astro-ph/9801307
- Yahil A., Strauss M.A., Davis M., Huchra J.P., 1991, ApJ, 372, 380